Monthly Notices of the ROYAL ASTRONOMICAL SOCIETY

MNRAS **509,** 4143–4148 (2022) https://doi.org/10.1093/mnras/stab3248
Advance Access publication 2021 November 10

Radio and X-ray spectral properties of gamma-ray bursts and pulsar wind nebulae

Bo-Tao Zhu,[1,2] Fang-Wu Lu,[3,2] Bing Zhou,[1,2] Jun Fang[2] and Li Zhang[2]★

[1]*College of Science, Yunnan Agricultural University, Kunming 650201, China*
[2]*Department of Astronomy, Key Laboratory of Astroparticle Physics of Yunnan Province, Yunnan University, Kunming 650091, China*
[3]*Department of Physics, Yuxi Normal University, Yuxi 653100, China*

Accepted 2021 November 1. Received 2021 November 1; in original form 2021 June 17

ABSTRACT

Both gamma-ray bursts (GRBs) and pulsar wind nebula (PWNe) are energetic outflows that are produced in powerful high-energy astrophysical environments. Based on the correlations between the radio luminosity L_R and X-ray luminosity L_X as well as between the multiband spectral slope α_{RX} and radio flux F_R for compiled GRB and PWN samples, the radio and X-ray spectral properties are statistically investigated. The results show that (1) the correlations between L_R and L_X are consistent for GRBs and PWNe, within the uncertainties; and (2) for the whole sample, F_R is related to α_{RX}, and GRBs have lower α_{RX} than PWNe. It may be concluded that GRBs and PWNe have the same or similar particle acceleration mechanisms and radiation processes, i.e. synchrotron radiation, to produce the radio-to-X-ray band emission.

Key words: methods: statistical – gamma-ray burst: general – pulsars: general – stars: winds, outflows.

1 INTRODUCTION

It is generally believed that gamma-ray bursts (GRBs) and pulsar wind nebulae (PWNe) have powerful outflows (e.g. Zhang & Mészáros 2004; Piran 2004; Mészáros 2006; Gaensler & Slane 2006). GRBs are the most powerful electromagnetic explosions in the universe, but their central engines are still debated (Zhang 2011). Possible central engines include stellar-mass black holes (Woosley 1993; Fryer, Woosley & Hartmann 1999) and neutron stars (Dai & Lu 1998; Zhang & Mészáros 2001). For PWNe, the central engines are neutron stars (Gaensler & Slane 2006). Although the central engines are different, there may be similar physical mechanisms in different outflow systems. Observations show that the signatures of non-thermal photons are revealed by power-law-form radiation spectra spanning an extremely wide range of wavelengths from radio to X-rays, and beyond. Thus, similar broad-band spectral energy distributions (SEDs) are critical to investigate the particle acceleration and radiation properties of GRBs and PWNe.

The SEDs of the prompt emission of GRBs are usually modelled by an empirical smoothly broken power-law function, i.e. the Band function (Band et al. 1993), but the origin is under debate. At present, the synchrotron-emission mechanism is the leading model (e.g. Mészáros, Rees & Papathanassiou 1994; Wang et al. 2009; Daigne et al. 2011; Zhang & Yan 2011). Other emission mechanisms, such as photosphere radiation (e.g. Mészáros et al. 2002; Rees & Mészáros 2005; Pe'er, Mészáros & Rees 2006) and the synchrotron self-Compton process (Racusin et al. 2008; Resmi & Zhang 2012), have also been proposed. However, the radiation mechanism of afterglows is well understood. It is generally believed that the observed afterglow radiation is well explained by synchrotron radiation (e.g. Sari, Piran & Narayan 1998; Panaitescu & Kumar 2001). The non-thermal radiation spectrum of a PWN consists of two components: the low-energy component (radio to X-ray bands) and high-energy component (MeV–TeV band). In general, the low-energy component is explained by the synchrotron radiation, and the high-energy component is produced by inverse Compton scattering (e.g. Atoyan & Aharonian 1996; Venter & de Jager 2007; Zhang, Chen & Fang 2008; Zhu, Fang & Zhang 2015; Zhu, Zhang & Fang 2018). In the process, the low-energy electrons radiate radio photons and the high-energy electrons emit X-ray band photons by synchrotron radiation, respectively.

It has been proposed that some physical mechanisms, like particle acceleration, magnetic field generation, and magnetic reconnection, may be the same or similar in different scale outflow systems (Bykov et al. 2012; Sironi, Keshet & Lemoine 2015). To explore similar physical mechanisms, correlations between the different physical quantities are studied in these outflow systems. For instance, the possible unified radiation mechanism was explored in GRBs and blazars with the L_P–E_P plane (Lyu et al. 2014), where L_P and E_P are the synchrotron peak luminosity and the corresponding photon energy, respectively; GRBs and blazers may have same synchrotron radiation mechanism by studying the correlations between the radio luminosity and broad-band spectral slope $\nu L_\nu(5\ \mathrm{GHz}) - \alpha_{RX}$, and the correlations between the radio luminosity and radio peak energy $\nu L_\nu(5\ \mathrm{GHz}) - \nu_{peak}$ (Wang, Yi & Dai 2014); evidence of the same energy-dissipation mechanisms is seen by studying the correlation between the jet power P_{jet} and intrinsic gamma-ray luminosity L_{jet} for blazars and GRBs (Nemmen et al. 2012; Zhang et al. 2013) as well as black hole X-ray binaries (BXBs) and low-luminosity active galactic nuclei (LLAGNs) (Ma, Xie & Hou 2014); and it has been found that the correlation between the jet power and gamma-ray luminosity of PWNe is consistent with the correlation

★ E-mail: lizhang@ynu.edu.cn

Table 1. PWNe data.

Source name	Associated pulsar	Distance kpc	F_R (5 GHz) Jy	F_X (2–10 keV) erg cm^{-2} s^{-1}	Γ_X	L_R (5 GHz) erg s^{-1}	L_X (2–10 keV) erg s^{-1}	References
3C 58	PSR J0205−6449	2.0	27.00	5.6×10^{-12}	2.07	6.46×10^{32}	2.68×10^{33}	(1), (2), (3)
Crab Nebula	PSR J0534−2200	2.0	680.00	2.1×10^{-8}	2.11	1.63×10^{34}	1.00×10^{37}	(4), (5)
N 157B	PSR J0537−6910	53.7	2.18	2.8×10^{-12}	2.43	3.76×10^{34}	9.66×10^{35}	(6), (7), (2)
N 158A	PSR B0540−69	50.0	0.06	5.4×10^{-12}	1.96	8.82×10^{32}	1.61×10^{36}	(8), (2)
Mouse	PSR J1747−2958	5.0	0.41	4.6×10^{-12}	1.93	6.11×10^{31}	1.37×10^{34}	(9), (2)
G292.0+1.8	PSR J1124−5916	6.2	3.50	6.8×10^{-12}	1.86	8.04×10^{32}	3.13×10^{34}	(10), (2)
G343.1−2.3	PSR B1706−44	2.7	0.03	4.0×10^{-13}	1.30	1.21×10^{30}	3.49×10^{32}	(11), (2)
G11.2−0.3	PSR J1811−1925	5.0	0.32	3.4×10^{-12}	1.70	4.78×10^{31}	1.02×10^{34}	(12), (2), (13)
Kes 75	PSR J1846−0258	6.0	0.25	2.2×10^{-11}	1.89	5.29×10^{31}	9.47×10^{34}	(14), (2), (15)
G34.7−0.4	PSR B1853+01	2.6	0.25	2.6×10^{-13}	2.20	1.00×10^{31}	2.10×10^{32}	(16), (2), (17)
G 54.1+0.3	PSR J1930+1852	6.0	0.32	5.4×10^{-12}	1.89	6.96×10^{31}	2.32×10^{34}	(18), (2), (19)
Boomerang	PSR J2229+6114	0.8	0.08	4.0×10^{-13}	1.00	3.05×10^{29}	3.06×10^{31}	(20), (21), (2)
Vela X	PSR J0835−4510	0.29	567	6.2×10^{-11}	1.52	2.85×10^{32}	6.23×10^{32}	(22), (2), (23)
HESS J1420−607	PSR J1420−6048	5.6	0.01	1.3×10^{-12}	2.30	2.20×10^{30}	4.87×10^{33}	(24), (25), (26)
MSH 15−52	PSR B1509−58	5.2	1.06	2.86×10^{-11}	2.05	1.71×10^{32}	9.25×10^{34}	(27), (28)
G21.5−0.9	PSR J1833−1034	4.7	6.54	4.0×10^{-11}	1.91	8.64×10^{32}	1.06×10^{35}	(29), (30), (31)
HESS J1813−178	PSR J1813−1749	4.8	0.36	5.6×10^{-12}	1.30	5.02×10^{31}	1.54×10^{34}	(32), (33), (34)
G76.9+1.0	PSR J2022−3842	10.0	0.43	4.0×10^{-14}	1.40	2.58×10^{32}	4.78×10^{32}	(35), (36), (7)
G310.6−1.6	PSR J1400−6325	7.0	0.11	1.51×10^{-11}	1.83	3.28×10^{31}	8.85×10^{34}	(37), (38)
CTA 1	PSR J0007+7303	1.4	11.60	1.2×10^{-11}	2.10	1.36×10^{32}	2.81×10^{33}	(39), (40), (41)
HESS J1356−645	PSR J1357−6429	2.5	0.54	7.9×10^{-12}	1.70	2.02×10^{31}	5.90×10^{33}	(42), (43), (44)
G0.9+0.1	PSR J1747−2809	13.3	1.45	5.78×10^{-12}	1.99	1.53×10^{33}	1.22×10^{35}	(45), (46)
HESS J1418−609	PSR J1418−6058	5.0	0.27	7.3×10^{-12}	1.50	4.02×10^{31}	2.18×10^{34}	(47), (25)
HESS J1640−465	PSR J1640−4631	10.5	3.10	5.5×10^{-13}	2.20	2.04×10^{33}	7.25×10^{33}	(48), (49), (50)
CTB 80	PSR B1951+32	2.0	35.6	5.1×10^{-12}	1.74	8.51×10^{32}	2.44×10^{33}	(51), (2)
G284.3−1.8	PSR J1016−5857	3.0	6.10	2.3×10^{-13}	0.90	3.28×10^{32}	2.48×10^{32}	(52), (2)
G319.9−0.7	PSR J1509−5850	2.6	0.43	1.5×10^{-13}	1.30	1.73×10^{31}	1.21×10^{32}	(53), (54)
DA 495		1.0	1.56	1.68×10^{-13}	2.00	9.34×10^{30}	2.01×10^{31}	(55), (56)
CTB 87		6.1	5.62	1.25×10^{-12}	1.68	1.25×10^{33}	5.56×10^{33}	(57), (58)

Note. References: (1) Green (1986), (2) Li, Lu & Li (2008), (3) Kothes (2016), (4) Macias-Pérez et al. (2010), (5) Willingale et al. (2001), (6) Lazendic et al. (2000), (7) Abdo et al. (2013), (8) Manchester, Staveley-Smith & Kesteven (1993), (9) Klingler et al. (2018), (10) Gaensler & Wallace (2003), (11) Giacani et al. (2001), (12) Tam, Roberts & Kaspi (2002), (13) Roberts et al. (2003), (14) Salter et al. (1989), (15) Leahy & Tian (2008), (16) Frail et al. (1996), (17) Petre, Kuntz & Shelton (2002), (18) Velusamy & Becker (1988), (19) Temim et al. (2017), (20) Becker, White & Edwards (1991), (21) Kothes et al. (2001), (22) Alvarez et al. (2001), (23) Dodson et al. (2003), (24) Van Etten & Romani (2010), (25) Ng, Roberts & Romani (2005), (26) Weltevrede et al. (2010), (27) Gaensler et al. (1999), (28) Gaensler et al. (2002), (29) Sun et al. (2011a), (30) Slane et al. (2000), (31) Camilo et al. (2006), (32) Brogan et al. (2005), (33) Helfand et al. (2007), (34) Halpern, Gotthelf & Camilo (2012), (35) Landecker, Higgs & Wendker (1993), (36) Arzoumanian et al. (2011), (37) Condon, Griffith & Wright (1993), (38) Renaud et al. (2010), (39) Sun et al. (2011b), (40) Slane et al. (1997), (41) Pineault et al. (1993), (42) HESS Collaboration (2011), (43) Izawa et al. (2015), (44) Lorimer et al. (2006), (45) Dubner, Giacani & Decourchelle (2008), (46) Porquet, Decourchelle & Warwick (2003), (47) Roberts et al. (1999), (48) Castelletti et al. (2011), (49) Gotthelf et al. (2014), (50) Lemiere et al. (2009), (51) Gao et al. (2011), (52) Milne et al. (1989), (53) Ng et al. (2010), (54) Hui & Becker (2007), (55) Kothes et al. (2008), (56) Coerver et al. (2019), (57) Kothes et al. (2020), (58) Matheson, Safi-Harb & Kothes (2013).

between the jet power and gamma-ray luminosity of GRBs, active galactic nuclei (AGNs), and BXBs (Zhu, Zhang & Fang 2019). Therefore, this likely indicates that the acceleration and emission or energy-dissipation mechanisms may be similar in all relativistic outflows regardless of their central engines. Recently, the standard synchrotron radiation model has been used to explain the broad-band non-thermal radiation spectra of GRBs and PWNe in the radio to X-ray bands (e.g. Xu, Yang & Zhang 2018; Xu et al. 2019; Xu 2019).

In this paper, we provide a new perspective and use the correlations between L_R and L_X, and α_{RX} and F_R to investigate the radio and X-ray spectral energy distribution properties of GRBs and PWNe. In Section 2, the sample of PWNe and GRBs is presented. In Section 3, the correlations between the radio luminosity L_R and X-ray luminosity L_X as well as between the radio flux F_R and the broad-band spectral slope α_{RX} are studied, respectively. Finally, our conclusions and discussions are presented in Section 4.

2 SAMPLES

Two samples are used: PWNe and GRBs.

The sample of PWNe is collected and listed in Table 1, which includes 29 PWNe. These PWNe are selected here according to the following criteria: (1) non-thermal emissions in the radio and X-ray bands are detected, and (2) the central pulsar in each PWN is known (except for CTB 87 and DA 495). For each PWN, the name of the PWN, the name of the central pulsar, and the distance are presented in columns 1, 2, and 3, respectively. The radio flux at 5 GHz (F_R) and X-ray flux in the 2–10 keV energy band (F_X), which have been directly observed or derived from the literature based on the radio and X-ray observations, are given in columns 4 and 5, respectively. The values of the photon spectral index Γ_X in the X-ray band are listed in column 6. Lastly, the radio luminosity L_R and the X-ray luminosity L_X are presented in columns 7 and 8, respectively.

For GRBs, a sample of radio afterglow observations was compiled by Chandra & Frail (2012); it consists of 304 GRBs with

Table 2. GRB data.

GRB	z	θ_j	$\log(L_{\rm jet}^{\rm R})$ erg s^{-1}	$\log(L_{\rm jet}^{\rm X})$ erg s^{-1}
970508	0.835	20.93	39.58	49.36
970828	0.958	5.15	37.83	48.14
980703	0.966	14.82	39.53	48.99
990510	1.619	3.36	38.10	48.90
021004	2.33	13.29	39.74	49.19
030226	1.986	3.43	38.09	47.75
030329	0.169	5.68	38.20	47.85
050416A	0.65	5.00	37.93	47.93
050603	2.821	5.00	38.99	49.67
050820A	2.615	5.07	38.56	48.44
050904	6.29	5.00	38.76	49.04
051022	0.809	5.00	37.93	48.49
060218	0.033	80.26	37.37	46.25
070125	1.548	7.90	39.42	49.74
071003	1.604	5.00	38.83	48.29
071010B	0.947	5.00	37.91	48.34
090323	3.57	4.63	38.88	49.39
090328	0.736	8.85	38.76	48.53
090423	8.26	9.64	39.28	50.25
090424	0.544	6.33	37.75	48.49
090715B	3	1.39	37.63	48.07
091020	1.71	5.00	38.68	48.73
100418A	0.62	8.43	38.37	47.43
100814A	1.44	5.00	38.56	48.12
991216	1.02	4.44	37.61	49.34
000210	0.85	5.02	37.52	48.71
050401	2.898	5.00	38.52	49.48
050525A	0.606	5.00	37.48	48.38
050824	0.83	5.00	37.71	47.39
060418	1.49	5.00	38.32	48.80
071020	2.146	5.00	38.39	48.76

radio observations. Since the X-ray flux declines quickly after the prompt emission, the X-ray flux at the prompt emission is usually approximated to the peak flux value. Thus, the X-ray luminosity in 2–10 keV is $L = 4\pi d_{\rm L}^2 P_{\rm bolo}$, where $P_{\rm bolo}$ is the bolometric peak flux, which is computed by the observed peak energy flux and Band function (for details, see Wang & Dai 2017). Meanwhile, the radio luminosities of GRBs are required. Therefore, the selected sample of GRBs should follow the criteria: (1) redshift is known, (2) radio and X-ray flux are measured, and (3) the peak energy and flux are observed. Based on these criteria and the sample compiled by Chandra & Frail (2012), 31 GRBs were collected by Wang & Dai (2017). Here the sample of 31 GRBs is used. For completeness, the name of each GRB, the redshift, and the intrinsic radio and X-ray luminosity are listed in Table 2, respectively. Note that the calculation processes of the intrinsic radio and X-ray luminosity are presented in detail in Wang & Dai (2017), and the value of the jet opening angle is from Chandra & Frail (2012) or Wang et al. (2014); this is estimated by the break time of the afterglow light-curve times (t_j) and number density (n) of the circumburst medium. Note that the X-ray prompt luminosities and radio afterglow luminosities of GRBs are used here. Previously some models predicted that the bright radio emission may be generated within seconds of the initial explosion of a GRB (e.g. Usov & Katz 2000; Sagiv & Waxman 2002). However, no evidence for GRB prompt radio emission detection has been confirmed so far. Thus, the afterglow radio luminosities of GRBs are used here. In fact, the time lags between X-ray and radio observations for our GRBs are from 1–50 d (Chandra & Frail 2012).

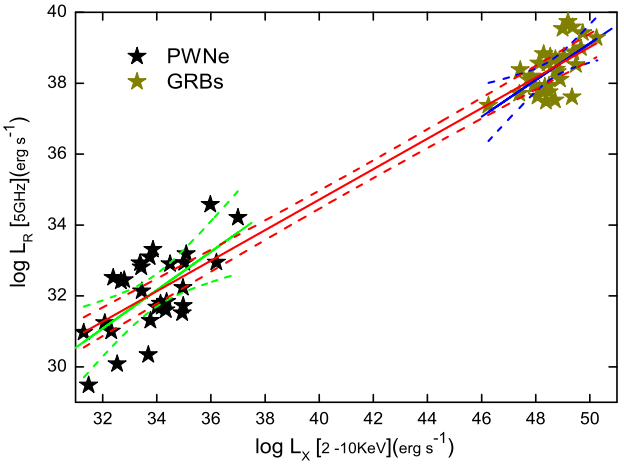

Figure 1. The correlations between $L_{\rm R}$ and $L_{\rm X}$ for GRBs and PWNe. The solid and dashed lines represent the best linear fits and their 3σ confidence bands for GRBs (blue), PWNe (green), and the whole sample (red), respectively.

3 RESULTS

To study the multiband SED properties of GRBs and PWNe in the radio–X-ray bands, the correlations between $L_{\rm R}$ and $L_{\rm X}$ and between $F_{\rm R}$ and $\alpha_{\rm RX}$ are investigated, respectively. In the process, the best linear fit $y = P_1 x + P_0$ to the data is used with the minimum χ^2 technique. For each fit, Pearson's correlation coefficient r and the probability of the null hypothesis $P_{\rm null}$ are calculated. It is generally believed that the correlation between two physical quantities is non-effective if $P_{\rm null} > 0.05$.

3.1 The $L_{\rm R}$–$L_{\rm X}$ correlation in GRBs and PWNe

The correlations between the luminosities $L_{\rm R}$ and $L_{\rm X}$ for the PWN and GRB samples were calculated, respectively. The results are shown in Fig. 1, and the best linear fitting results are given by

$$\log L_{\rm R}^{\rm GRB} = (13.29 \pm 5.85) + (0.52 \pm 0.12) \log L_{\rm X}^{\rm GRB}, \quad (1)$$

for GRBs, and

$$\log L_{\rm R}^{\rm PWN} = (13.74 \pm 4.20) + (0.54 \pm 0.12) \log L_{\rm X}^{\rm PWN}, \quad (2)$$

for PWN, where Pearson's correlation coefficient is $r_{\rm ab} = 0.62$ and 0.64 and the probability of the null hypothesis $P_{\rm null} \sim 1.81 \times 10^{-4}$ and $\sim 1.63 \times 10^{-4}$ for GRBs and PWNe, respectively. From equations (1) and (2), it can be concluded that the two correlations are consistent within the uncertainties. For the whole sample (GRBs + PWNe), the best-fitting result is

$$\log L_{\rm R} = (17.50 \pm 0.53) + (0.43 \pm 0.01) \log L_{\rm X}\ , \quad (3)$$

where $r_{\rm ab} = 0.98$ and $P_{\rm null} \sim 0$. Comparing this with equations (1) and (2), the correlation coefficient has an obvious enhancement after adding the GRB or PWN sample, and the related results are shown in Fig. 1. In the process, since the X-ray and radio emissions of GRBs are highly beamed (Rhoads 1997), following Wang et al. (2014) or Wang & Dai (2017), the isotropic luminosity should be corrected by $L_{\rm jet} = L_{\rm iso} F_{\rm beam}$, where $F_{\rm beam} = 1 - \cos\theta_j$, $L_{\rm iso}$ is the isotropic luminosity, and $F_{\rm beam}$ is the beaming factor. While PWNe are extended sources, radio and X-ray emission is not highly beamed. Therefore, the beaming effect is ignored. Note that the luminosities in equations (1)–(3) are in the units of erg s^{-1}.

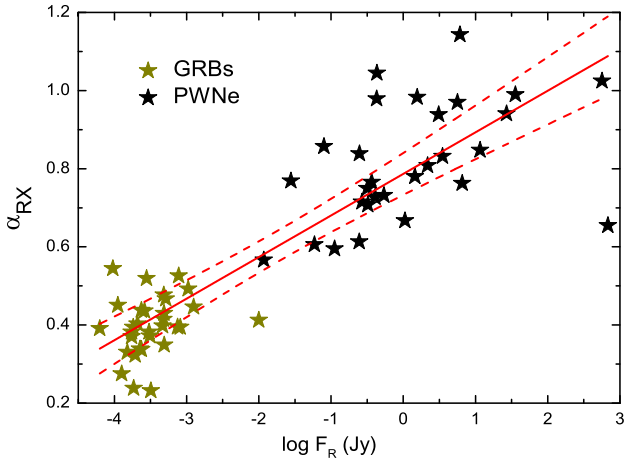

Figure 2. The correlation between α_{RX} and F_R. The red solid and dashed lines represent the best linear fit and the 3σ confidence band for the whole sample.

3.2 The correlation α_{RX}–F_R in GRBs and PWNe

Motivated by the research into the correlation between the broad-band spectral slope α_{RX} and the radio luminosity at 5 GHz in some outflow systems (Fossati et al. 1998; Wang et al. 2014), the correlation between the broad-band spectral slope α_{RX} and the radio flux at 5 GHz F_R is studied for GRB and PWN systems, respectively. The broad-band spectral slope α_{RX} is defined as

$$\alpha_{RX} = -\frac{\log(f_{\nu_R}/f_{\nu_X})}{\log(\nu_R/\nu_X)}, \quad (4)$$

where $\nu_R = 5$ GHz and $\nu_X = 1$ keV. The X-ray flux, f_{ν_X}, at 1 keV can be obtained based on X-ray band observations. Since the signature of the non-thermal photon spectrum is revealed by a power law, the X-ray flux, F_X, in the X_{low}–X_{up} keV band is written as

$$\int_{X_{low,keV}}^{X_{up,keV}} A_X \nu^{-\alpha_X} d\nu = F_X. \quad (5)$$

In general, the X-ray flux usually evolves as $\nu^{-P/2}$ with the power-law $P = 2.2$ index of the photon distribution for GRBs (Sari et al. 1998). Similar to Wang et al. (2014), $\alpha_X = 1.1$ is applied, and the X-ray flux at 0.3–10 keV, F_X, is listed in table 1 of Chandra & Frail (2012). The flux at 1 keV, f_{ν_X}, can be derived by obtaining the value of A_X. Like GRBs, based on the relevant parameters of Table 1, the flux at 1 keV can be derived for PWNe. Note that $\alpha_X = \Gamma_X - 1.0$ for PWNe, and the corresponding Γ_X are listed in Table 1.

As shown in Fig. 2, the correlations between F_R and α_{RX} are researched for the GRBs and PWNe, respectively. There is no evidence that α_{RX}–F_R is related (correlation coefficient $r_{ab} = 0.23$ with a probability of $P_{null} = 0.2$) for the sample of GRBs, and α_{RX}–F_R is only mildly correlated for the pure PWNe sample (correlation coefficient $r_{ab} = 0.46$ with a probability of $P_{null} = 0.01$). These results prevent us from comparing the correlations of the GRBs with PWNe. However, F_R and α_{RX} are correlated for the whole sample (GRBs and PWNe). The best-fitting result is given by

$$\alpha_{RX} = (0.78 \pm 0.02) - (0.10 \pm 0.01) \log F_R\ , \quad (6)$$

where $r_{ab} = 0.88$ and $P_{null} \sim 0$. In addition, GRBs occupy a lower-α_{RX} region than PWNe.

4 CONCLUSION AND DISCUSSION

GRBs and PWNe are two population sources with relativistic outflows in the universe, and many of their physical properties are similar. In this paper, based on a sample of 29 PWNe and 31 GRBs with radio and X-ray observations, the radio and X-ray spectral properties of GRBs and PWNe are statistically studied by using the correlations between L_R and L_X and between α_{RX} and F_R. Our results show that the slope of the L_R–L_X correlation is 0.52 ± 0.12 for GRBs, which is consistent with 0.54 ± 0.12 for PWNe. The whole sample follows $L_R \sim L_X^{0.43\pm0.01}$, and PWNe occupy a lower-luminosity region than GRBs (see Fig. 1). The correlations not only provide further evidence for the similarities in GRBs and PWNe but also make possible a new physical analogy to understand the radiation mechanism of the GRB.

As described in Section 2, the radio afterglow luminosities and X-ray prompt luminosities of GRBs are used. It is generally believed that the X-ray prompt emission and radio afterglow emission of GRBs come from different particle populations. Theoretically, the afterglow of GRBs is produced by synchrotron radiation of particles accelerated by external shock (Mészáros & Rees 1997; Sari et al. 1998) and the prompt emission is produced by particles accelerated by internal shocks or magnetic reconnection (e.g. Rees & Mészáros 1994; Daigne & Mochkovitch 1998; Zhang & Yan 2011), but the prompt emission mechanism is still highly debated for GRBs. Similarly, there are two different particle populations that could produce the synchrotron radiation spectrum of PWNe (e.g. Atoyan & Aharonian 1996; Zhu et al. 2015; Lyutikov et al. 2019; Luo et al. 2020). Some particles are considered to be accelerated at the pulsar wind termination shock of the equatorial portion (e.g. Rees & Gunn 1974; Kennel & Coroniti 1984a, b; Atoyan & Aharonian 1996) and these particles emit X-ray-band photons by synchrotron emission, while other particles are accelerated in the light cylinder of the pulsar or reconnecting current sheets of the bulk of the nebula (e.g. Atoyan & Aharonian 1996; Olmi et al. 2014; Lyutikov et al. 2019; Luo et al. 2020) and these particles produce radio-band photons by synchrotron emission. Thus, if a correlation between L_R and L_X exists in GRBs and PWNe, the prompt radiation mechanism of GRBs is argued to be synchrotron emission, and the acceleration processes of particles may be the same or similar in GRBs and PWNe.

As shown in Fig. 2, there is no strong correlation between α_{RX} and F_R for GRBs or PWNe, which prevents us from comparing the GRB correlations with those of PWNe. For the whole sample (GRBs+PWNe), however, there is a strong correlations between α_{RX} and F_R, and $\alpha_{RX} \propto F_R^{0.1}$. Moreover, GRBs occupy a lower-α_{RX} region than PWNe. The following interpretation of the different regions is possible. In general, the average magnetic field strength of the emitting region is between 10^{-2} and 10^2 G for GRBs (Burgess et al. 2020), while the average magnetic field strength is between 1 and 10^2 μG for PWNe (Torres et al. 2014; Zhu et al. 2018). The different magnetic fields may result in the GRB occupation of a lower-α_{RX} region than PWNe.

ACKNOWLEDGEMENTS

We would like to thank the anonymous referee for the very constructive comments. This work is partially supported by the National Key R&D Program of China under grant No. 2018YFA0404204, the National Natural Science Foundation of China (NSFC U1738211, 11803027, 11873042, and U2031107), and Yunnan Fundamental Research Projects (grant No. 202101AU070099).

DATA AVAILABILITY

The data underlying this paper will be shared on reasonable request to the corresponding author.

REFERENCES

Abdo A. A. et al., 2013, ApJS, 208, 17
Alvarez H., Aparici J., May J., Reich P., 2001, A&A, 372, 636
Arzoumanian Z., Gotthelf E. V., Ransom S. M., Safi-Harb S., Kothes R., Landecker T. L., 2011, ApJ, 739, 39
Atoyan A. M., Aharonian F. A., 1996, MNRAS, 278, 525
Band D. et al., 1993, ApJ, 413, 281
Becker R. H., White R. L., Edwards A. L., 1991, ApJS, 75, 1
Brogan C. L. et al., 2005, ApJ, 629, 105
Burgess J. M. et al., 2020, Nat. Astron., 4, 174
Bykov A., Gehrels N., Krawczynski H.,Lemoine M., Pelletier G., Pohl M., 2012, Space Sci. Rev., 173, 309
Camilo F., Ransom S. M., Gaensler B. M., Slane P.O., Lorimer D. R., Reynolds J., Manchester R. N., Murray S. S., 2006, ApJ, 637, 456
Castelletti G., Giacani E., Dubner G., Joshi B. C., Rao A. P., Terrier R., 2011, A&A, 536, A98
Chandra P., Frail D. A., 2012, ApJ, 746, 156
Coerver A. et al., 2019, ApJ, 878, 126
Condon J. J., Griffith M. R., Wright A. E., 1993, AJ, 106, 1095
Dai Z. G., Lu T., 1998, A&A, 333, L87
Daigne F., Mochkovitch R., 1998, MNRAS, 296, 275
Daigne F. et al., 2011, A&A, 526, A110
Dodson R., Legge D., Reynolds J. E., McCulloch P. M., 2003, ApJ, 596, 1137
Dubner G., Giacani E., Decourchelle A., 2008, A&A, 487, 1033
Fossati G., Maraschi L., Celotti A., Comastri A., Ghisellini G., 1998, MNRAS, 299, 433
Frail D. A., Giacani E. B., Goss W. M., Dubner G., 1996, ApJ, 464, L165
Fryer C. L., Woosley S. E., Hartmann D. H., 1999, ApJ, 526, 152
Gaensler B. M., Slane P. O., 2006, ARA&A, 44, 17
Gaensler B. M., Wallace B. J., 2003, ApJ, 594, 326
Gaensler B. M., Brazier K. T. S., Manchester R. N., Johnston S., Green A. J., 1999, MNRAS, 305, 724
Gaensler B. M., Arons J., Kaspi V. M., Pivovaroff M. J., Kawai N., Tamura K., 2002, ApJ, 569, 878
Gao X. Y., Han J. L., Reich W., Reich P., Sun X. H., Xiao L., 2011, A&A, 529, A159
Giacani E. B., Frail D. A., Goss W. M., Vieytes M., 2001, AJ, 121, 3133
Gotthelf E. V. et al., 2014, ApJ, 788, 155
Green D. A., 1986, MNRAS, 218, 533
Halpern J. P., Gotthelf E. V., Camilo F., 2012, ApJ, 753, L14
Helfand D., Gotthelf E. V., Halpern J. P., Camilo F., Semler D. R., Becker R. H., White R. L., 2007, ApJ, 665, 1297
HESS Collaboration, 2011, A&A, 533, A103
Hui C. Y., Becker W., 2007, A&A, 470, 965
Izawa M., Dotani T., Fujinaga T., Bamba A., Ozaki M., Hiraga J. S., 2015, PASJ, 67, 43
Kennel C. F., Coroniti F. V., 1984a, ApJ, 283, 694
Kennel C. F., Coroniti F. V., 1984b, ApJ, 283, 710
Klingler N., Kargaltsev O., Pavlov G. G., Ng C.-Y., Beniamini P., Volkov I., 2018, ApJ, 861, 5
Kothes R., 2016, Supernova Remnants: An Odyssey in Space after Stellar Death. p. 46. Available at: http://snr2016.astro.noa.gr
Kothes R. et al., 2001, ApJ, 560, 236
Kothes R., Landecker T. L., Reich W., Safi-Harb S., Arzoumanian Z., 2008, ApJ, 687, 516
Kothes R. et al., 2020, MNRAS, 496, 723
Landecker T. L., Higgs L. A., Wendker H. J., 1993, A&A, 276, 522
Lazendic J. S., Dickel J. R., Haynes R. F., Jones P. A., White G. L., 2000, ApJ, 540, 808
Leahy D. A., Tian W., 2008, A&A, 480, L25
Lemiere A., Slane P., Gaensler B. M., Murray S., 2009, ApJ, 706, 1269
Li X.-H., Lu F.-J., Li Z., 2008, ApJ, 682, 1166
Lorimer D. R. et al., 2006, MNRAS, 372, 777
Luo Y., Lyutikov M., Temim T., Comisso L., 2020, ApJ, 896, 147
Lyu F., Liang E.-W., Liang Y.-F., Wu X.-F., Zhang J., Sun X.-N., Lu R.-J, 2014, ApJ, 793, 36
Lyutikov M., Temim T., Komissarov S., Slane P., Sironi L., Comisso L., 2019, MNRAS, 489, 2403
Ma R. Y., Xie F. G., Hou S. J., 2014, ApJ, 780, L14
Macias-Pérez J. F., Mayet F., Aumont., Désert F.-X., 2010, ApJ, 711, 417
Manchester R. N., Staveley-Smith L., Kesteven M. J., 1993, ApJ, 411, 756
Matheson H., Safi-Harb S., Kothes R., 2013, ApJ, 774, 33
Mészáros P., 2006, Rep. Prog. Phys., 69, 2259
Mészáros P., Rees M. J., 1997, ApJ, 476, 232
Mészáros P., Rees M. J., Papathanassiou H., 1994, ApJ, 432, 181
Mészáros P., Ramirez-Ruiz E., Rees M. J., Zhang B., 2002, ApJ, 578, 812
Milne D. K., Caswell J. L., Kesteven M. J.,Haynes R. F., Roger R. S., 1989, Publ. Astron. Soc. Australia, 8, 187
Nemmen R. S., Georganopoulos M., Guiriec S., Meyer E. T., Gehrels N., Sambruna R. M., 2012, Science, 338, 1445
Ng C.-Y., Roberts M. S. E., Romani R. W., 2005, ApJ, 627, 904
Ng C.-Y., Gaensler B., Chatterjee S., Johnston S., 2010, ApJ, 712, 596
Olmi B., Del Zanna L., Amato E., Bandiera R., Bucciantini N., 2014, MNRAS, 438, 1518
Panaitescu A., Kumar P., 2001, ApJ, 560, L49
Pe'er A., Mészáros P., Rees M. J., 2006, ApJ, 642, 995
Petre R., Kuntz K. D., Shelton R. L., 2002, ApJ, 579, 404
Pineault S., Landecker T. L., Madore B., Gaumont-Guay S., 1993, AJ, 105, 1060
Piran T., 2004, Rev. Mod. Phys., 76, 1143
Porquet D., Decourchelle A., Warwick R. S., 2003, A&A, 401, 197
Racusin J. L. et al., 2008, Nature, 455, 183
Rees M. J., Gunn J. E., 1974, MNRAS, 167, 1
Rees M. J., Mészáros P., 1994, ApJ, 430, L93
Rees M. J., Mészáros P., 2005, ApJ, 628, 847
Renaud M. et al., 2010, ApJ, 716, 670
Resmi L., Zhang B., 2012, MNRAS, 426, 1385
Rhoads J. E., 1997, ApJ, 487, L1
Roberts M. S. E., Romani R. W., Johnston S., Green A. J., 1999, ApJ, 515, 712
Roberts M. S. E., Tam C. R., Kaspi V. M., Lyutikov M., Vasisht G., Pivovaroff M., Gotthelf E. V., Kawai N., 2003, ApJ, 588, 992
Sagiv A., Waxman E., 2002, ApJ, 574, 861
Salter C. J., Reynolds S. P., Hogg D. E., Payne J. M., Rhodes P. J., 1989, ApJ, 338, 171
Sari R., Piran T., Narayan R., 1998, ApJ, 497, L17
Sironi L., Keshet U., Lemoine M., 2015, Space Sci. Rev., 191, 519
Slane P., Seward F. D., Bandiera R., Torii K., Tsunemi H., 1997, ApJ, 485, 221
Slane P., Chen Y., Schulz N. S., Seward F. D., Hughes J. P., Gaensler B. M., 2000, ApJ, 533, L29
Sun X. H., Reich P., Reich W., Xiao L., Gao X. Y., Han J. L., 2011a, A&A, 536, A83
Sun X. H., Reich W., Wang C., Han J. L., Reich P., 2011b, A&A, 535, A64
Tam C., Roberts M. S. E., Kaspi V. M., 2002, ApJ, 572, 202
Temim T.,, et al, 2017, ApJ, 836, 129
Torres D. F., Cillis A., Martín J., de Oña Wilhelmi E., 2014, J. High Energy Astrophys., 1, 31
Usov V. V., Katz J. I., 2000, A&A, 364, 655
Van Etten A., Romani R. W., 2010, ApJ, 711, 1168
Velusamy T., Becker R. H., 1988, AJ, 95, 1162
Venter C., de Jager O. C., 2007, in Becker W., Huang H.-H., eds, MPE Report 291, Proc. 363rd WE-Heraeus Seminar on Neutron Stars and Pulsars. Max Planck Institut für extraterrestrische Physik, Garching, p. 40
Wang F. Y., Dai Z. G., 2017, MNRAS, 470, 1101
Wang X.-Y., Li Z., Dai Z.-G., Mészáros P., 2009, ApJ, 698, L98
Wang F. Y., Yi S. X., Dai Z. G., 2014, ApJ, 786, L8
Weltevrede P. et al., 2010, ApJ, 708, 1426

Willingale R., Aschenbach B., Griffiths R. G., Sembay S., Warwick R. S., Becker W., Abbey A. F., Bonnet-Bidaud J.-M., 2001, A&A, 365, L212
Woosley S. E., 1993, ApJ, 405, 273
Xu S., 2019, J. Phys. Conf. Ser., 1332, 012019
Xu S., Yang Y.-P., Zhang B., 2018, ApJ, 853, 43
Xu S., Klingler N., Kargaltsev O., Zhang B., 2019, ApJ, 872, 10
Zhang B., 2011, Comptes Rendus Phys., 12, 206
Zhang B., Mészáros P., 2001, ApJ, 552, L35
Zhang B., Mészáros P., 2004, Int. J. Modern Phys. A, 19, 2385
Zhang B., Yan H., 2011, ApJ, 726, 90
Zhang L., Chen S. B., Fang J., 2008, ApJ, 676, 1216
Zhang J., Liang E. W., Sun X. N., Zhang B., Lu Y., Zhang S.-N., 2013, ApJ, 774, L5
Zhu B. T., Fang J., Zhang L., 2015, MNRAS, 451, 3145
Zhu B. T., Zhang L., Fang J., 2018, A&A, 609, A110
Zhu B. T., Zhang L., Fang J., 2019, ApJ, 873, 120

This paper has been typeset from a TEX/LATEX file prepared by the author.